Journal of Digital Imaging (2019) 32:987–994
https://doi.org/10.1007/s10278-019-00195-2

Assessment of Orbital Computed Tomography (CT) Imaging Biomarkers in Patients with Thyroid Eye Disease

Shikha Chaganti[1,2] · Kevin Mundy[3] · Michael P. DeLisi[4] · Katrina M. Nelson[5] · Robert L. Harrigan[5] · Robert L. Galloway[4] · Bennett A. Landman[1,4,5] · Louise A. Mawn[3]

Published online: 13 June 2019
© Society for Imaging Informatics in Medicine 2019

Abstract
To understand potential orbital biomarkers generated from computed tomography (CT) imaging in patients with thyroid eye disease. This is a retrospective cohort study. From a database of an ongoing thyroid eye disease research study at our institution, we identified 85 subjects who had both clinical examination and laboratory records supporting the diagnosis of thyroid eye disease and concurrent imaging prior to any medical or surgical intervention. Patients were excluded if imaging quality or type was not amenable to segmentation. The images of 170 orbits were analyzed with the developed automated segmentation tool. The main outcome measure was to cross 25 CT structural metrics for each eye with nine clinical markers using a Kendall rank correlation test to identify significant relationships. The Kendall rank correlation test between automatically calculated CT metrics and clinical data demonstrated numerous correlations. Extraocular rectus muscle metrics, such as the average diameter of the superior, medial, and lateral rectus muscles, showed a strong correlation ($p < 0.05$) with loss of visual acuity and presence of ocular motility defects. Hertel measurements demonstrated a strong correlation ($p < 0.05$) with volumetric measurements of the optic nerve and other orbital metrics such as the crowding index and proptosis. Optic neuropathy was strongly correlated ($p < 0.05$) with an increase in the maximum diameter of the superior muscle. This novel method of automated imaging metrics may provide objective, rapid clinical information. This data may be useful for appreciation of severity of thyroid eye disease and recognition of risk factors of visual impairment from dysthyroid optic neuropathy from CT imaging.

Keywords CT · Multi-atlas · Thyroid eye disease · Optic nerve

Introduction

Early diagnosis and recognition of orbital involvement in thyroid eye disease are important for appropriate treatment and management. However, due to the variable clinical presentation and reliance upon subjective tests such as visual acuity testing, both the presence and severity of disease can elude diagnosis. An objective metric that correlates strongly with functional limitations, impending optic nerve dysfunction, or other causes of significant visual impairment could be valuable in supporting a decision to intervene and potentially prevent orbital complications and visual loss.

Presently, computed tomography (CT) imaging is the most readily available imaging modality to evaluate the orbit for evidence of thyroid eye disease [1]. Previous authors have investigated CT metrics as an objective finding to be used as a tool in aiding early diagnosis. The extraocular muscle, bone, fat, and orbital volume indices are among the CT characteristics that have been studied in the past [2–16]. However, the methods used in these studies have included manual freehand drawing of orbital structures on multiple image planes. The data acquisition and volume calculations are often sufficiently cumbersome to preclude their routine clinical use. The commercially available segmentation programs such as MIMICS

✉ Shikha Chaganti
shikha.chaganti@vanderbilt.edu

[1] Department of Computer Science, Vanderbilt University, 2301 Vanderbilt Place, Nashville, TN 37235, USA

[2] Vanderbilt University, 371 Jacobs Hall, Nashville, TN 37235, USA

[3] Vanderbilt Eye Institute, Vanderbilt University School of Medicine, 2311 Pierce Avenue, Nashville, TN 37232, USA

[4] Department of Biomedical Engineering, Vanderbilt University, Nashville, TN 37235, USA

[5] Department of Electrical Engineering, Vanderbilt University, Nashville, TN 37235, USA

and MAXILLO involve laborious calculations and lack consistency between users [17, 18]. As of yet, no study has used an automated method of orbital volumetric analysis in orbital disease. We have developed an automated method for analyzing orbital anatomic structures. The purposes of the present study are to apply the method of automatically generating orbital metrics from CT imaging to a cohort of thyroid eye disease patients and investigate their relationships with recorded clinical characteristics such as the ocular motility defects, Hertel measurements, visual function measures, and presence of optic neuropathy.

Methods

A retrospective review at an academic center from January 1, 2000, to January 1, 2012, identified 381 patients; 102 of these patients met the clinical criteria for thyroid eye disease and had available CT imaging of the orbits. Of these, 85 clinical patients were selected for the study after excluding 10 patients due to imaging issues, such as severe artifact and low resolution, and 7 due to the fact that the available scans in the electronic database were after decompression surgery. Institutional Review Board approval was obtained at Vanderbilt University prospectively to evaluate both the clinical and imaging data of the 381 patients and store them in RedCAP and XNAT databases. Clinical characteristics including the date of diagnosis, sex, age, ocular motility, Hertel exophthalmometer measurements, smoking history, visual acuity, and color vision testing were recorded.

CT Data

Patients underwent CT imaging of the orbits as part of the regular clinical care. For each of the 85 selected patients, the highest resolution scan pre-decompression surgery was manually selected. Although variable imaging protocols (CT head, orbital, maxillofacial, etc.) were acquired, for all imaging scans, the field of view included the globes and full optic nerves from the globes to the chiasm.

Image Processing

For each patient, the selected CT image was loaded into eXtensible Neuroimaging Archive Toolkit [19, 20] and automatically processed with segmentation software to identify the extents of the optic nerves (including surrounding CSF sheathes), extraocular rectus muscles, globes, and orbital fat and calculate clinically relevant measurements from these structures. This process consists of three main steps: multi-atlas segmentation, Kalman tracking of extraocular muscles, and metric computation.

The first step involves segmentation of the globe, the optic nerve, the extraocular muscles, and the orbital fat using the multi-atlas paradigm. This step automatically identifies structures of interest in a new scan based on example scans with expert labels known as atlases. The process includes a manual element, i.e., preparation of the example atlases that requires an expert to demarcate orbital structures in about 20 CT scans taking about ~ 2 h per scan. However, this is a one-time process only, and once a set of labeled atlases are prepared, they can be used for all future analyses at no additional manual cost. The remainder of the image processing pipeline is fully automated.

Since the images analyzed in this paper are clinically acquired, there is a lot of variability in imaging protocols which include the CT head, orbital, and maxillofacial. Therefore, the first step of the automated process is localization of the orbit in the target scan. Each of the atlases is rigidly registered to the target space using Deeds registration [21]. The average of all the rigidly labeled atlases is computed at each voxel. A region of interest is cropped around voxels that have at least a probability of 0.5 to ascertain the approximate location of the eye orbit in the target scan. Next, each of the atlases is non-rigidly registered to the cropped target image using ANTs SyN registration with a cross-correlation metric [22], with the aim of achieving a voxel-wise correspondence between the target scan and the example atlases. Finally, non-local statistical label fusion [23] is used to combine the label estimates at each voxel to obtain the final labels in the target scan. The globe, the optic nerve, and the extraocular muscles are identified through this process.

However, identifying individual extraocular muscles through this process is challenging, especially in the case of thyroid eye disease, since there is orbital crowding due to inflammation of the muscles. We use Kalman filters to segment each of the orbital muscles. Kalman filters are used to track the muscles from the front of the orbit, where they are well separated, to the orbital apex. The centroids of the four extraocular muscles and the globe are computed at the coronal slice at the center of the globe, where the muscles are well separated. Kalman filters are used to track the centroids across coronal slices. A watershed algorithm is used at each coronal slice to get the muscle labels, based on the Kalman centroid estimates as seed points. A detailed explanation of this method is provided by Chaganti et al. [24]. The Dice similarity coefficient for segmented structures was 0.77, which was comparable to human reproducibility of 0.73.

Finally, descriptive features of the orbital anatomy were computed for each patient from the segmentations to assess correlations with clinical characteristics. These features were based on previous work in manual CT measurements for thyroid eye disease. Some of the metrics that were previously calculated for two-dimensional slices were expanded for three-dimensional volumes, for example, the volumetric crowding index. The complete list of 25 features or orbital structural metrics included the (1–13) volume, maximum

diameter, and average diameter for the superior, inferior, medial, and lateral rectus muscles and total recti muscle volume [5, 6, 11, 25, 26]; (14) Barrett muscle index [8]; (15–16) volume and diameter of the globe [10, 26–28]; (17) orbital volume; (18) volume crowding index; (19) orbital angle; (20) degree of proptosis [29]; (21) length along the optic nerve;(22–25) traditional length, volume, average area, and maximum diameter of the optic nerve [30, 31].

All structural metrics were performed bilaterally, which resulted in 25 measures for each eye. Figure 1 illustrates the image processing workflow from a CT scan to segmentation to derived metrics.

Clinical Data

For each patient, clinical characteristics associated with severity of the disease such as Hertel exophthalmometer measurements [32, 33], ocular motility defects [6], and presence of optic neuropathy [4, 34] were recorded along with age, sex, and smoking history [35, 36]. The threshold for ocular motility defects was greater than 25% limitation in any meridian of eye movement. Although the literature regarding optic nerve compromise in thyroid eye disease has included vague and loosely defined criteria for optic neuropathy, a clear and unequivocal definition of optic neuropathy was chosen to most robustly associate clinical and imaging features. Subjects were classified as having optic neuropathy if they had documented decreased visual acuity, decreased visual field, decreased color vision (30% or more), nerve fiber layer edema, and/or imaging studies that demonstrate signs of orbital nerve compression. A visual field defect was defined as present if a cluster of at least 3 points on one side of the horizontal meridian, each depressed by at least 5 dB from the normal values for age. The defect was considered to be mild if the pattern mean defect was −2 to −7 dB, moderate if −7 to 14 dB, and severe if 14 to 30 dB. In addition, measures of visual function that were shown to be associated with thyroid eye disease and dysthyroid optic neuropathy [33, 37], such as the best corrected visual acuity, logMAR visual acuity, AMA-defined visual acuity, and field scores, were calculated as described by Rondinelli et al. [38], and measures of color vision were recorded. In total, nine clinical measures were recorded. For 82 patients, the clinical data was obtained at the time of the CT scan. Three of the patients had no visual field testing available at the time of the scan, so the closest available formal testing within 6 months was obtained and confirmed the confrontation field at the time of the scan.

Statistical Analysis

A Kendall rank correlation test [39] was used to identify significant relationships between the nine clinical characteristics and the 25 structural metrics for each eye, which were automatically calculated from the CT images. Outlier points are removed for each metric and clinical measure pair, by retaining those values that fall within two standard deviations of the mean. Next, z-score normalization was performed and correlation between the metric and clinical measures was computed. This correlation is known as the Kendall tau coefficient.

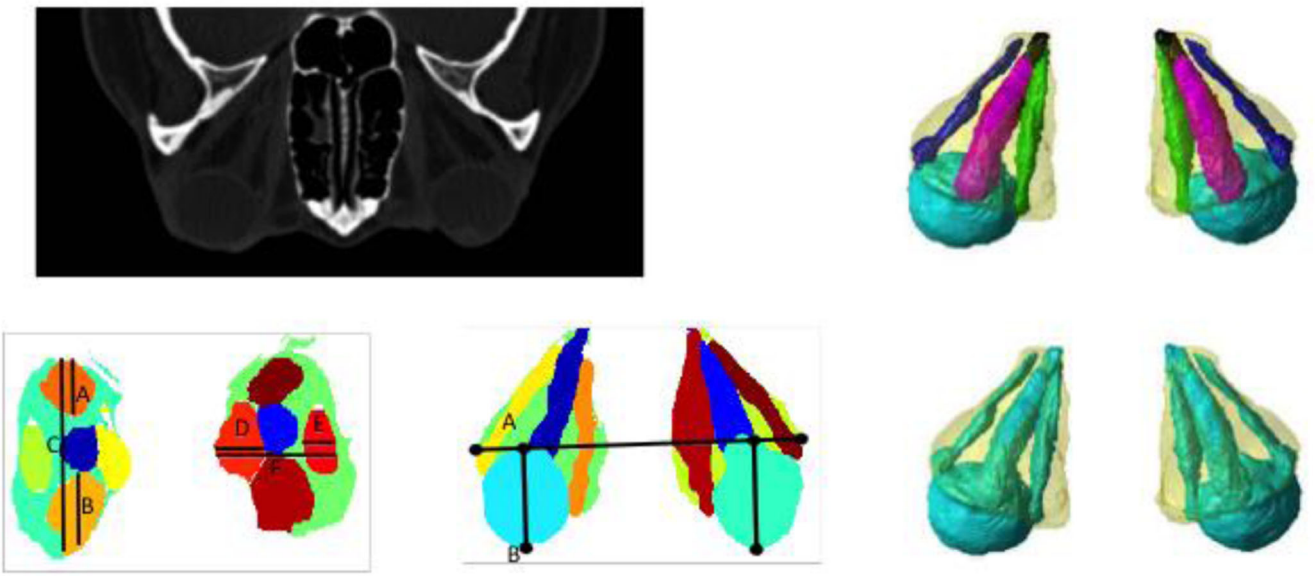

Fig. 1 Pipeline for automatic CT image analysis. Top left indicates the original clinically acquired CT scan. Top right shows 3-D rendering of orbital structures automatically identified using the multi-atlas method. We segment the globe, optic nerve, extraocular rectus muscles, and orbital fat. Bottom left shows Barrett's index metric, calculated as max(A + B/C,(D + E)/F) for each eye. Bottom center shows the degree of proptosis metric, calculated as the anterior displacement of the eye globe from the interzygomatic line, i.e., AB. Bottom right shows the volumetric crowding index metric, calculated as the ratio between the volumes of soft tissue and fat in the orbit

Table 1 Univariate Kendall rank correlations between extraocular muscle metrics and clinical covariates

	Superior muscle volume	Inferior muscle volume	Lateral muscle volume	Medial muscle volume	Superior muscle average diameter	Inferior muscle average diameter	Lateral muscle average diameter	Medial muscle average diameter	Superior muscle maximum diameter	Inferior muscle maximum diameter	Lateral muscle maximum diameter	Medial muscle maximum diameter	Total muscle volume
LogMAR visual acuity	0.05	−0.04	0.07	0.03	0.06	0.08	0.06	0.06	0.10	0.04	0.07	0.06	0.06
Color vision (rato)	−0.08	0.02	0.04	−0.05	0.00	−0.02	0.03	−0.08	−0.12*	−0.10	0.02	−0.08	0.00
Smoking (0 no, 2 current, 1 former)	0.01	0.10*	0.13**	0.05	0.02	0.11*	0.11*	0.04	−0.02	0.13**	0.13**	0.01	0.09
Motility defect (1 no, 2 yes)	0.10	0.15**	0.11*	0.10	0.14**	0.17**	0.13**	0.09	0.12*	0.21**	0.12*	0.03	0.14**
Hertel ophthalmometer measurement	−0.16**	−0.03	0.05	0.02	−0.06	0.02	0.04	0.00	−0.01	0.07	0.05	−0.01	0.02
Optic neuropathy (1 no, 2 yes)	0.05	−0.04	0.07	−0.03	0.09	0.00	0.06	0.02	0.16**	0.04	0.11*	−0.06	0.04
Best corrected visual acuity (denominator)	0.11	0.02	−0.01	0.11	0.13	−0.02	0.00	0.20**	0.08	0.00	0.03	0.08	0.03
Visual acuity score	−0.13	−0.04	−0.04	−0.18**	−0.12	−0.01	−0.05	−0.24**	−0.07	−0.05	−0.09	−0.14*	−0.08
Functional acuity score	−0.15**	−0.04	−0.06	−0.20**	−0.17**	0.00	−0.09	−0.26**	−0.11	−0.15**	−0.17**	−0.12	−0.10
Visual field score	−0.06	−0.02	−0.14*	−0.12	−0.05	−0.05	−0.14*	−0.15*	−0.02	−0.06	−0.11	−0.08	−0.10
Functional field score	−0.10	0.08	−0.07	−0.03	−0.13	0.07	−0.07	−0.07	−0.10	0.01	−0.10	0.02	−0.04
Functional vision score	−0.14*	0.01	−0.02	−0.17**	−0.17**	0.07	−0.03	−0.22**	−0.11	−0.09	−0.12	−0.08	−0.06

**$p < 0.05$; *$p < 0.1$

A rank correlation test is used in this work as it is a non-parametric test that measures the significance of the rankings of the measures instead of the absolute values. Therefore, it identifies monotonic relationships even when they are non-linear, which makes it an ideal test for clinical data [40]. Kendall tau coefficients that had a p value of less than 0.05 were considered to be strongly significant, and those with a p value of less than 0.1 were considered to be moderately significant.

Results

Eighty-five patients between the ages of 18 and 83 (48.9 ± 13.56) meeting the clinical criteria for thyroid eye disease who also had CT imaging related to their condition were retrospectively selected in our data set. Of these patients, 63 were female (74%). Seventy-five (88%) of these were hyperthyroid, six (7%) were euthyroid, and four (5%) hypothyroid. The cohort has 32 current smokers, 10 former smokers, and 43 non-smokers. Nine of the 85 patients had optic neuropathy (2 patients had decreased color and acuity; 1 had decreased color and field; 5 had decreased acuity, color, and field; and 1 had nerve fiber layer edema and decreased acuity and field).

The automatic segmentation rendered labels of the structures defined in the atlas including the globe, the optic nerve, the inferior, medial, superior, and lateral rectus muscles, and the orbital fat as seen in the top right of Fig. 1. The structural metrics examined included the volume, length, and diameter measurements for all the segmented structures shown in the top right of Fig. 1, as well as Barrett's muscle index as seen in the bottom left of Fig. 1, degree of proptosis as seen in the bottom middle of Fig. 1, and volumetric crowding index as seen in the bottom right of Fig. 1. A univariate Kendall rank correlation test demonstrated a variety of correlations between CT metrics and clinical data.

Table 1 shows the rank correlations between the clinical characteristics and structural measurements of the extraocular muscles (EOM). A strong correlation was seen between loss of visual function and EOM metrics. Medial muscle volume and diameter were negatively correlated with the visual acuity score ($p < 0.05$) and functional acuity score ($p < 0.05$). Superior muscle volume was negatively correlated with the functional acuity score ($p = 0.048$). Color vision measurements demonstrated a negative correlation, i.e., the larger the muscle, the worse the color vision, with a superior rectus maximum diameter ($p < 0.05$). Ocular motility deficit also demonstrated a strong positive correlation with EOM metrics including inferior rectus volume ($p = 0.02$), superior ($p = 0.03$), inferior ($p = 0.01$), and lateral ($p = 0.05$) rectus muscle average diameter, inferior rectus muscle maximum diameter ($p < 0.05$), total muscle volume ($p = 0.03$), and Barrett's muscle index ($p < 0.05$).

Table 2 Univariate Kendall rank correlations between orbital and optic nerve metrics and clinical covariates

Rho values	Barrett index	Globe volume	Globe diameter	On length	On traditional length	On volume	On average area	On maximum diameter	Orbital volume	Volumetric crowding index	Proptosis	Angle
LogMAR visual acuity	0.03	0.06	0.05	−0.01	−0.08	0.03	0.08	0.00	−0.04	0.14**	−0.06	0.09
Color vision (rato)	0.09	−0.06	−0.06	0.05	0.03	0.10	0.02	−0.01	−0.04	0.03	0.16**	−0.08
Smoking (0 no, 2 current, 1 former)	0.07	0.00	−0.01	0.03	0.07	−0.03	−0.11*	−0.09	0.09	−0.16**	0.22**	0.02
Motility defect (1 no, 2 yes)	0.21**	0.13**	0.12*	−0.01	−0.02	0.02	0.01	0.04	0.16**	−0.02	0.00	0.00
Hertel ophthalmometer measurement	−0.10	−0.03	−0.03	0.15**	0.26**	−0.11*	−0.17**	−0.19**	0.24**	−0.24**	0.24**	0.15**
Optic neuropathy (1 no, 2 yes)	0.04	−0.05	−0.05	−0.10	−0.08	−0.09	−0.07	−0.10	−0.01	−0.10	−0.03	0.00
Best corrected visual acuity (denominator)	0.03	0.10	0.10	−0.11	−0.15*	0.21**	0.25**	0.16**	0.01	0.17**	−0.08	0.09
Visual acuity score	−0.07	−0.08	−0.08	0.09	0.11	−0.24**	−0.27**	−0.15*	0.01	−0.14*	0.11	−0.07
Functional acuity score	−0.16**	−0.04	−0.04	0.11	0.12	−0.16**	−0.19**	−0.12	−0.04	−0.14*	0.07	−0.09
Visual field score	−0.06	−0.03	−0.03	0.14*	0.09	−0.12	−0.13*	−0.05	0.14*	−0.07	−0.03	−0.15*
Functional field score	0.04	−0.06	−0.06	0.18**	0.16**	0.03	0.02	0.05	0.01	0.08	−0.04	−0.14*
Functional vision score	−0.09	−0.05	−0.05	0.14*	0.14*	−0.09	−0.11	−0.09	−0.05	−0.11	0.02	−0.13*

**$p < 0.05$; *$p < 0.1$

Table 2 shows the correlations between clinical characteristics and other orbital metrics, including volumetric measurements of the optic nerve. Hertel measurements demonstrated a strong positive correlation with traditional optic nerve length ($p \ll 0.05$), full optic nerve length ($p < 0.05$), orbital volume ($p \ll 0.05$), and proptosis ($p \ll 0.05$) and demonstrated a negative correlation with optic nerve average area ($p < 0.05$), optic nerve maximum diameter ($p < 0.05$), and volumetric crowding index ($p \ll 0.05$).

Smoking history demonstrated a positive correlation with degree of proptosis measured on CT ($p \ll 0.05$), inferior muscle volume ($p = 0.09$), lateral rectus muscle volume ($p = 0.03$), inferior muscle average diameter ($p = 0.09$), inferior muscle maximum diameter ($p = 0.01$), lateral rectus muscle maximum diameter ($p = 0.04$) and demonstrated a negative correlation with the volumetric crowding index ($p = 0.01$).

Discussion

Dysthyroid optic neuropathy is the most feared and devastating consequence of thyroid eye disease. Unfortunately, several of the clinical markers that are indicative of optic nerve damage may have confounding variables or be subjective in nature such that their utility in identifying dysthyroid optic neuropathy may be particularly limited in certain situations. Delay in diagnosis may lead to permanent vision loss. An objective marker of impending orbital compromise including extent of muscle involvement or, even more importantly, a dysthyroid optic neuropathy risk metric that may be obtained rapidly could have tremendous clinical implications. The current study investigates the relationship between CT imaging and dysthyroid optic neuropathy and factors closely associated with it such as loss of visual acuity, visual field defects, and color vision [41]. It also investigates the relationship between CT imaging and other characteristics shown to be associated with thyroid eye disease in the previous literature such as ocular motility defects, proptosis (Hertel measurements), and smoking history.

The significance of this study is that we have developed an automated method to segment structures of interest and extract volumetric and structural metrics related to visual function from clinically acquired imaging. This contrasts with previously published methods of segmentation that are often cumbersome, require significant manual effort, and due to these factors are not applicable in a fast-paced clinical setting. Analysis of data obtained by this method within a population of individuals with thyroid eye disease reveals several correlations with potential for clinical significance. Imaging reports of high risk of optic neuropathy would be especially helpful. This is most clinically relevant for those patients with quiet, tightly packed orbits—our data have shown us that it is not the highly proptotic patients (stretched optic nerve) but rather the large-packed muscle patients who are at greatest risk of vision loss from thyroid eye disease. Ideally, a seasoned clinician would correctly identify that a patient's decreased visual acuity and color vision is related to thyroid eye disease; however, some of the patients including our large cohort of thyroid patients had their human lens removed and were not sent for tertiary care until after the cataract surgery. This work will be used to help develop a positive and negative predictive probability.

The present data set reinforces the importance of Hertel measurements in patients with thyroid eye disease as it correlates strongly with radiographic evidence of pathologic optic nerve changes as well as more complex indices of orbital crowding such as the negative association seen to the volumetric crowding index. Clinically, Hertel measurements correlated strongly with radiographic proptosis.

Optic neuropathy was associated with increased superior and lateral muscle diameters, possibly indicative of optic nerve compression. The small sample size of patients with clinical evidence of optic neuropathy is a likely contributor to the absence of other statistically significant correlations in the present study. Nevertheless, the strong correlation demonstrated by several clinical visual function metrics such as visual acuity, visual field defects, and color vision with automatically obtained orbital metrics serves as evidence that this new method of obtaining objective radiographic data may provide clinically relevant early evidence of risk that could prevent permanent vision loss from dysthyroid optic neuropathy and potentially from other causes of optic neuropathy.

Acknowledgments This work was conducted in part using the resources of the Advanced Computing Center for Research and Education at Vanderbilt University, Nashville, TN.

Funding/Support This study is supported in part by an unrestricted grant from the Vanderbilt Eye Institute and Physician Scientist Award from Research to Prevent Blindness, New York, NY. This project was supported by the NIH 1R03EB012461 and the National Center for Research Resources, Grant UL1 RR024975-01 (now at the National Center for Advancing Translational Sciences, Grant 2 UL1 TR000445-06). This research was supported by NSF CAREER 1452485 and NIH grants 5R21EY024036. This research was conducted with the support from Intramural Research Program, National Institute on Aging, NIH. This project was supported in part by ViSE/VICTR. This work was also supported by the National Institutes of Health in part by the National Institute of Biomedical Imaging and Bioengineering training grant T32-EB021937.

Compliance with Ethical Standards Institutional Review Board approval was obtained at Vanderbilt University prospectively to evaluate both the clinical and imaging data of the 381 patients and store them in RedCAP and XNAT databases.

Conflict of Interest The authors declare that they have no conflict of interest.

Disclaimer The content is solely the responsibility of the authors and does not necessarily represent the official views of the NIH.

References

1. Muller-Forell W, Kahaly GJ: Neuroimaging of Graves' orbitopathy. Best Pract Res Clin Endocrinol Metab 26:259–271, 2012
2. Kennerdell JS, Rosenbaum AE, El-Hoshy MH: APical optic nerve compression of dysthyroid optic neuropathy on computed tomography. Archives of Ophthalmology 99:807–809, 1981
3. Feldon SE, Weiner JM: Clinical significance of extraocular muscle volumes in graves; ophthalmopathy: a quantitative computed tomography study. Archives of Ophthalmology 100:1266–1269, 1982
4. Barrett L, Glatt HJ, Burde RM, Gado MH: Optic nerve dysfunction in thyroid eye disease: CT. Radiology 167:503–507, 1988
5. Hallin ES, Feldon SE: Graves' ophthalmopathy: I. Simple CT estimates of extraocular muscle volume. British Journal of Ophthalmology 72:674–677, 1988
6. Hallin ES, Feldon SE: Graves' ophthalmopathy: II. Correlation of clinical signs with measures derived from computed tomography. The British Journal of Ophthalmology 72:678–682, 1988
7. Giaconi JA, Kazim M, Rho T, Pfaff C: CT scan evidence of dysthyroid optic neuropathy. Ophthalmic Plastic & Reconstructive Surgery 18:177–182, 2002
8. Monteiro MLR, Gonçalves ACP, Silva CTM, Moura JP, Ribeiro CS, Gebrim EMMS: Diagnostic ability of Barrett's index to detect dysthyroid optic neuropathy using multidetector computed tomography. Clinics 63:301–306, 2008
9. Chan LL, Tan HE, Fook-Chong S, Teo TH, Lim LH, Seah LL: Graves ophthalmopathy: the bony orbit in optic neuropathy, its apical angular capacity, and impact on prediction of risk. AJNR. American journal of neuroradiology 30:597–602, 2009
10. Weis E, Heran MKS, Jhamb A, Chan AK, Chiu JP, Hurley MC et al.: Quantitative computed tomographic predictors of compressive optic neuropathy in patients with thyroid orbitopathy: a volumetric analysis. Ophthalmology 119:2174–2178, 2012
11. Weis E, Heran MS, Jhamb A et al.: Clinical and soft-tissue computed tomographic predictors of dysthyroid optic neuropathy: refinement of the constellation of findings at presentation. Archives of Ophthalmology 129:1332–1336, 2011
12. Gonçalves ACP, Silva LN, Gebrim EMMS, Monteiro MLR: Quantification of orbital apex crowding for screening of dysthyroid optic neuropathy using multidetector CT. AJNR. American journal of neuroradiology 33:1602–1607, 2012
13. Al-Bakri M, Rasmussen AK, Thomsen C, Toft PB: Orbital volumetry in Graves' orbitopathy: muscle and fat involvement in relation to dysthyroid optic neuropathy. ISRN ophthalmology 2014:435276, 2014
14. Lima B d R, Perry JD: Superior ophthalmic vein enlargement and increased muscle index in dysthyroid optic neuropathy. Ophthalmic Plastic & Reconstructive Surgery 29:147–149, 2013
15. Gonçalves ACP, Silva LN, Gebrim EMMS, Matayoshi S, Monteiro MLR: Predicting dysthyroid optic neuropathy using computed tomography volumetric analyses of orbital structures. Clinics 67:891–896, 2012
16. Feldon SE, Lee CP, Muramatsu SK, Weiner JM: Quantitative computed tomography of Graves ophthalmopathy. Extraocular muscle and orbital fat in development of optic neuropathy. Arch Ophthalmol 103:213–215, 1985
17. Potgieser PW, Regensburg NI, Wiersinga WM, Mourits MP: Re: computer-aided analysis of orbital volume: a novel technique. Ophthal Plast Reconstr Surg 30:72, 2014
18. Strong EB, Chahal HS: Reply Re:Computer-aided analysis of orbital volume: a novel technique. Ophthal Plast Reconstr Surg 30: 72–73, 2014
19. Harrigan RL, Yvernault BC, Boyd BD, Damon SM, Gibney KD, Conrad BN et al.: Vanderbilt University Institute of Imaging Science Center for Computational Imaging XNAT: a multimodal data archive and processing environment. Neuroimage 124:1097–1101, 2016
20. Marcus DS, Olsen TR, Ramaratnam M, Buckner RL: The extensible neuroimaging archive toolkit: an informatics platform for managing, exploring, and sharing neuroimaging data. Neuroinformatics 5:11–34, Spring, 2007
21. Heinrich MP, Jenkinson M, Brady M, Schnabel JA: MRF-based deformable registration and ventilation estimation of lung CT. IEEE Transactions on Medical Imaging 32:1239–1248, 2013
22. Avants BB, Epstein CL, Grossman M, Gee JC: Symmetric diffeomorphic image registration with cross-correlation: evaluating automated labeling of elderly and neurodegenerative brain. Medical Image Analysis 12:26–41, 2008
23. Asman AJ, Landman BA: Non-local statistical label fusion for multi-atlas segmentation. Medical Image Analysis 17:194–208, 2013
24. S. Chaganti, K. Nelson, K. Mundy, Y. Luo, R. L. Harrigan, S. Damon, et al., Structural functional associations of the orbit in thyroid eye disease: Kalman filters to track extraocular rectal muscles. in *Proceedings of SPIE–the International Society for Optical Engineering*, 2016.
25. Ozgen A, Ariyurek M: Normative measurements of orbital structures using CT. AJR. American Journal of Roentgenology 170: 1093–1096, 1998
26. Szucs-Farkas Z, Toth J, Balazs E, Galuska L, Burman KD, Karanyi Z et al.: Using morphologic parameters of extraocular muscles for diagnosis and follow-up of Graves' ophthalmopathy: diameters, areas, or volumes? *AJR. American journal of roentgenology* 179: 1005–1010, 2002
27. Tian S, Nishida Y, Isberg B, Lennerstrand G: MRI measurements of normal extraocular muscles and other orbital structures. Graefes Arch Clin Exp Ophthalmol 238:393–404, May 2000
28. Pearce E, Bridge H: Is orbital volume associated with eyeball and visual cortex volume in humans? Ann Hum Biol 40:531–540, 2013
29. Nugent RA, Belkin RI, Neigel JM, Rootman J, Robertson WD, Spinelli J et al.: Graves orbitopathy: correlation of CT and clinical findings. Radiology 177:675–682, 1990
30. Rubin PA, Watkins LM, Rumelt S, Sutula FC, Dallow RL: Orbital computed tomographic characteristics of globe subluxation in thyroid orbitopathy. Ophthalmology 105:2061–2064, 1998
31. Peyster RG, Hoover ED, Hershey BL, Haskin ME: High-resolution CT of lesions of the optic nerve. AJR Am J Roentgenol 140:869–874, May 1983
32. Hales I, Rundle F: Ocular changes in Graves' disease. QJM 29: 113–126, 1960
33. Mourits M, Koornneef L, Wiersinga W, Prummel M, Berghout A, Van Der Gaag R: Clinical criteria for the assessment of disease activity in Graves' ophthalmopathy: a novel approach. British Journal of Ophthalmology 73:639–644, 1989
34. Neigel JM, Rootman J, Belkin RI, Nugent RA, Drance SM, Beattie CW, Spinelli JA: Dysthyroid optic neuropathy: the crowded orbital apex syndrome. Ophthalmology 95:1515–1521, 1988
35. Lazarus JH: Epidemiology of Graves' orbitopathy (GO) and relationship with thyroid disease. Best Practice & Research Clinical Endocrinology & Metabolism 26:273–279, 2012
36. Thornton J, Kelly S, Harrison R, Edwards R: Cigarette smoking and thyroid eye disease: a systematic review. Eye 21:1135–1145, 2007
37. L. Wartofsky, Classification of Eye Changes of Graves-Disease. Ed: Mary Ann Liebert Inc Publ 2 Madison Avenue, Larchmont, NY 10538, 1992.

38. R. D. Rondinelli, E. Genovese, and C. R. Brigham, Guides to the Evaluation of Permanent Impairment: American Medical Association, 2008.
39. Abdi H: The Kendall rank correlation coefficient. In: Encyclopedia of Measurement and Statistics. Thousand Oaks, CA: Sage, 2007, pp. 508–510
40. Mukaka M: A guide to appropriate use of correlation coefficient in medical research. Malawi Medical Journal 24:69–71, 2012
41. McKeag D, Lane C, Lazarus JH, Baldeschi L, Boboridis K, Dickinson AJ, Hullo AI, Kahaly G, Krassas G, Marcocci C, Marino M, Mourits MP, Nardi M, Neoh C, Orgiazzi J, Perros P, Pinchera A, Pitz S, Prummel MF, Sartini MS, Wiersinga WM: Clinical features of dysthyroid optic neuropathy: a European Group on Graves' Orbitopathy (EUGOGO) survey. British Journal of Ophthalmology 91:455–458, 2007

Publisher's Note Springer Nature remains neutral with regard to jurisdictional claims in published maps and institutional affiliations.